Radiation Physics and Chemistry 188 (2021) 109644

Contents lists available at ScienceDirect

Radiation Physics and Chemistry

journal homepage: www.elsevier.com/locate/radphyschem

A mechanistic approach towards the formation of bityrosine in proteins by ionizing radiation – GYG model peptide

Sebastian Sowiński [a,*], Gustavo H.C. Varca [a,b,**], Sławomir Kadłubowski [a], Ademar B. Lugão [b], Piotr Ulański [a]

[a] Institute of Applied Radiation Chemistry (IARC), Faculty of Chemistry, Lodz University of Technology, Wroblewskiego 15, 93-590, Lodz, Poland
[b] Instituto de Pesquisas Energéticas e Nucleares (IPEN-CNEN/SP), Av. Prof. Lineu Prestes, n° 2242, Cidade Universitária, 05508-000, São Paulo, SP, Brazil

ARTICLE INFO

Keywords:
Mechanism
Ionizing radiation
Pulse radiolysis
GYG tripeptide
Bityrosine
Protein crosslinking

ABSTRACT

One of the methods of protein crosslinking used in the synthesis of protein-based nanoparticles is the formation of bityrosine bridges, which may be achieved by the recombination of phenoxyl-type radicals in irradiated protein solutions. Radiation-induced formation of phenoxyl radicals in tyrosine is promoted in presence of H^+. In this work, kinetics of this process and the influence of pH were studied by pulse radiolysis measurements of a model peptide H-Gly-Tyr-Gly-OH (GYG), which may help to solve questions raised for bigger, more complex systems in comparable conditions. The main route of phenoxyl radicals formation consists of the addition reaction of hydroxyl radical to the phenol ring on the tyrosine side-chain and proton catalyzed water molecule elimination. A similar effect was observed in studies of tripeptide solutions containing phosphate buffer. The presented data include time-resolved optical spectroscopy of transient species formed under pulse electron beam irradiation and a comparison of the kinetics of the phenoxyl radicals formation in samples at various pH and in presence of phosphate buffer. The postulated mechanism and obtained values of rate constants of the formation and decay of transient species were additionally checked by simple probabilistic simulations.

1. Introduction

Protein-based nanoparticles represent a potential group of therapeutic agents applied for biomedical research. Globular proteins and proteolytic enzymes, e.g. bovine serum albumin and papain, have been studied at the nanoscale (Varca et al., 2014; Queiroz et al., 2016) and demonstrated high potential for drug delivery due to the tunable nanoparticle size, biological affinity among other biopharmaceutical advantages (Amri and Mamboya, 2012) which are not observed nor expected in the case of inorganic molecules and more advanced than in polymeric materials meant for biomedical applications.

For instance, papain (EC 3.4.22.2) is a proteolytic enzyme extracted from the latex of *Carica Papaya Linnaeus* with a well-defined structure (Kamphuis et al., 1984) and a high potential for drug delivery (Varca et al., 2016; Fazolin et al., 2020), as this enzyme holds desirable properties for wound treatment (Amri and Mamboya, 2012) due to its anti-inflammatory and antitumoral characteristics (Müller et al., 2016).

The use of ionizing radiation for the synthesis of polymer-based nanoparticles has been demonstrated over the years and proven effective for a wide variety of substrate molecules (Ulański et al., 1998; Ulanski and Rosiak, 2004; An et al., 2011; Dispenza et al., 2012; Varca et al., 2014; Duygu Sütekin and Güven, 2019; Matusiak et al., 2020). When it comes to proteins and protein-like structures, the use of high-energy radiation combined with cosolvents like ethanol and methanol may promote crosslinking and sterilization simultaneously, depending upon the dose, and has been successfully applied towards

* Corresponding author. Institute of Applied Radiation Chemistry (IARC), Faculty of Chemistry, Lodz University of Technology, Wroblewskiego 15, 93-590, Lodz, Poland.
** Corresponding author. Instituto de Pesquisas Energéticas e Nucleares (IPEN-CNEN/SP), Av. Prof. Lineu Prestes, n° 2242, Cidade Universitária, 05508-000, São Paulo, SP, Brazil.
E-mail addresses: ssowinski@mitr.p.lodz.pl (S. Sowiński), varca@alumni.usp.br (G.H.C. Varca).

https://doi.org/10.1016/j.radphyschem.2021.109644
Received 5 February 2021; Received in revised form 8 June 2021; Accepted 10 June 2021
Available online 15 June 2021

achieving protein-based nanoparticles with controllable particle size and preserved bioactivity or biological function (Soto Espinoza et al., 2012; Queiroz et al., 2016; Fazolin et al., 2020).

On the other hand, high-energy radiation may affect the biomolecules by direct or indirect effects and can impair the biological function of proteins as well as their tridimensional structure (Saha et al., 1995). In principle, biomolecules are prone to attack by radiation via indirect effects to a major extent through the action of free radicals generated as a function of water/solvent radiolysis. This exposition leads to damage and depending upon the conditions may trigger the formation of several protein-protein crosslinks which contribute significantly to the conformational changes and the newly acquired structure within the protein. Among those, disulfide bridges, bityrosines, and other linkages have been studied, identified, and hypothesized (Giulivi et al., 2003; Houée-Levin and Bobrowski, 2013; Bian and Chowdhury, 2014; Hägglund et al., 2018).

The mechanism of bityrosine formation, perhaps one of the most relevant cross-linking types identified in papain (Varca et al., 2014) and BSA (Queiroz et al., 2016), occurs via three main stages: abstraction of hydrogen (with the formation of phenoxyl radical), recombination and isomerization (Giulivi et al., 2003). The formation of Tyr-Tyr linkages occurs when the oxidizing species derived from water radiolysis, e.g. hydroxyl radical, lead to protein crosslinking mainly via tyrosine residues (Queiroz et al., 2016). The hypothesis behind the mechanism involved in the nanoparticle formation is evidence of crosslinking formation by C–O–C bonds induced by the hydroxyl radical (Heinecke et al., 1993; Saha et al., 1995). The nature of such linkages plays an important role in the nanoparticle formation, whereas the intermolecular bonding is characterized by the increase in molecular weight due to the linkages with another molecule and intramolecular one does not present any change (Ulański et al., 2002).

The formation of phenoxyl radicals is the first step in the process of tyrosine-mediated crosslinking. In aqueous solutions of proteins and peptides, phenoxyl radicals on tyrosine (TyrO$^{\bullet}$) are formed as one of the products of reaction with hydroxyl radicals (Fig. 1). Most of the hydroxyl radicals reacting with tyrosine undergo addition to aromatic ring in meta- (reaction 1) and ortho- (reaction 2) positions, forming dihydroxyhexadienyl radicals ($^{\bullet}$TyrOH). A small fraction of hydroxyl radicals is known to cause the formation of phenoxyl radicals without observable intermediate product (reaction 3). The main route of phenoxyl radicals formation is proton-catalyzed water elimination (reaction 4). This reaction is known to occur only from ortho-adducts (o-$^{\bullet}$TyrOH). Another product of tyrosine solutions radiolysis is dihydroxyphenylalanine (DOPA), being a product of disproportionation and recombination reactions (reactions 5, 6), that compete with the water elimination process. Kinetics of mentioned processes and factors influencing them seem of great importance in terms of bityrosine formation (Solar et al., 1984). Those three processes amount to about 90% of radicals formed on tyrosine in reaction with hydroxyl radical (Getoff, 1992), other processes being primarily relatively slow reactions with main-chain of the amino acid. While possible, other adducts to side-chain group of tyrosine (on C1 and C4) are not observable spectroscopically and therefore it is not possible to experimentally confirm their contribution to reactions in this system.

Cysteine bonding is another linkage that was also postulated to take place in the crosslinking process via disulfide bridges (Gaber, 2005). The

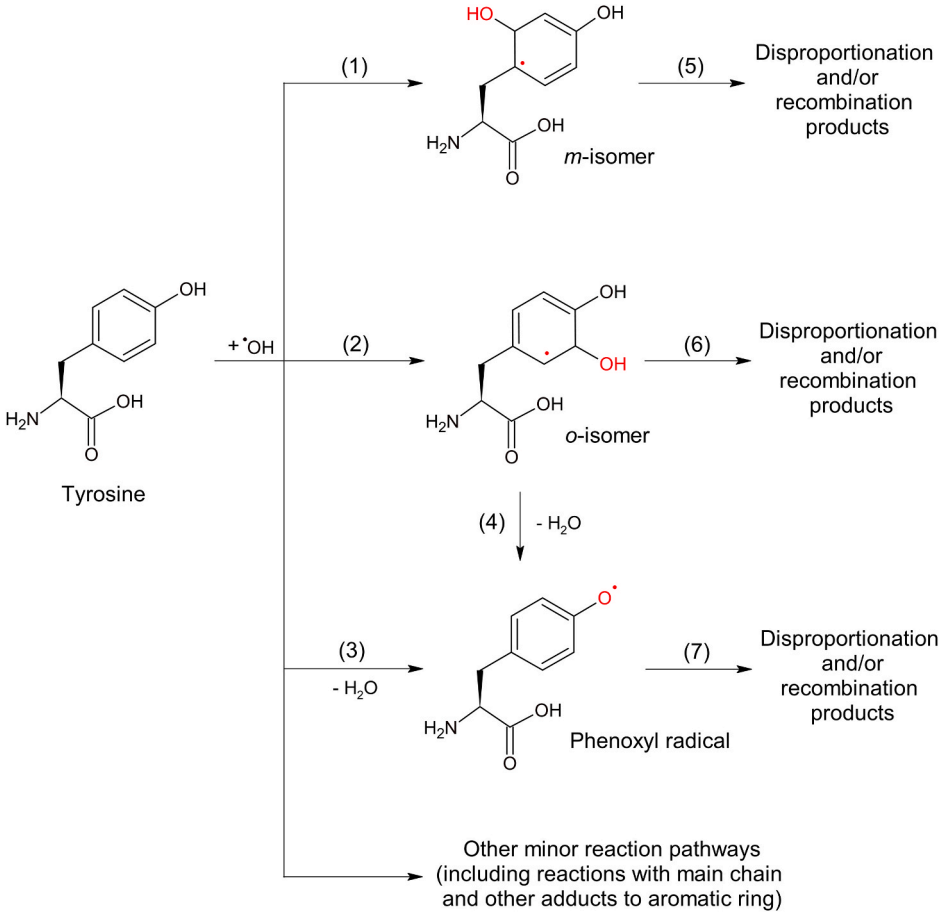

Fig. 1. Mechanism of hydroxyl radical reaction with tyrosine (inspired by Getoff, 1992).

Cys-Cys and cysteine thiyl are derivates of the free cysteine residues attacked by oxidizing species and depending upon the condition may bind to another thiol to build up a disulfide bridge (Houée-Levin and Bobrowski, 2013).

Regardless of several types of crosslinking which have been postulated, it does vary from protein to protein and the crosslinking method. When it comes to radiation-induced reaction pathways, there is limited knowledge not allowing a proper understanding of the radiation chemistry aspects and pathways for the formation of such crosslinks even in terms of what is the major type of crosslinking and the possible role of each one of them.

Although special attention to this matter has been given in the last decade, the mechanism of nanoparticle formation has not been thoroughly established yet and remains a theme of future studies. Within this context, this paper aims to provide a radiation-chemistry approach for better understanding of the mechanism beneath the formation of such crosslinks, particularly directed towards the synthesis of papain-based nanoparticles. H-Gly-Tyr-Gly-OH (GYG) tripeptide was chosen as low-molecular-weight model for more complex protein systems, being more realistic analogue of the protein system than tyrosine itself and allowing to follow selectivity of the reaction with tyrosine residue, but on the other hand reducing the complexity of multitude of reactions and transients encountered when complete protein molecule is irradiated. Such an approach was also intended to indicate if replacing the carboxyl and amino terminal functions in tyrosine by peptide bonds does influence the reaction pathways and kinetics known from earlier works on pure tyrosine. Kinetic study of this compound in conditions similar to the ones used for proteins in synthesis of nanoparticles provided insight into processes involved in radiation- induced crosslinking of proteins via bityrosine formation, especially regarding the influence of phosphate buffer on formation of phenoxyl radicals on tyrosine. Kinetic simulations have been applied to confirm the mechanistic scheme.

2. Materials and methods

2.1. Materials and samples preparation

Peptide H-Gly-Tyr-Gly-OH (GYG, M = 295.3 g mol^{-1}) (>99%, Bachem, Germany) was used as received. Peptide solutions were prepared with deionized water (conductivity ≈ 10 μS/m, produced with TKA-Millipore system). Peptide solutions in water were confirmed to have pH = 5.4 in the used range of concentrations. More acidic conditions were obtained by the addition of perchloric acid (Sigma-Aldrich). The phosphate buffer used in the experiments was obtained by dissolving dibasic sodium phosphate (Sigma-Aldrich) and monobasic sodium phosphate (Sigma Aldrich) in 1:1 M ratio, so that the pH = 7.0. In the case of all samples, pH was determined using Radiometer Copenhagen PHM 95 pH-meter. Samples were saturated for 40 min with N_2O (99%, medical-grade, Linde) or with argon (99.99%, Linde, Poland) prior to the measurements. Nitrous oxide was additionally purged from a trace amount of oxygen with the use of an alkaline pyrogallol bath. 10 mM solutions of tert-butanol (99+%, Merck) were used in the experiments involving hydroxyl radical scavenger. Potassium thiocyanate (99+%, A.C.S. grade) used for dosimetry of ionizing radiation was purchased from Sigma-Aldrich.

2.2. Pulse radiolysis

A nanosecond pulse radiolysis system with spectrophotometric detection has been used in all of the conducted measurements. The setup is based on the 6 MeV linear electron accelerator (ELU-6a, Eksma, Russia), 17 ns electron pulses were used in the study. The detection system consisted of 50 W xenon lamp, monochromator (Spectra Pro 275, Princeton Instruments), photomultiplier (Hamamatsu), and digital oscilloscope (Tektronix TDS540). A water filter has been used to remove IR part of the lamp spectrum. Further details regarding the pulse radiolysis setup were described elsewhere (Karolczak et al., 1992). Measurements were conducted in quartz cuvettes with an optical path of 10 mm. The total sample volume for the pulse radiolysis experiment was 30 ml, samples were mixed between measurements to minimize the effects of potential peptide degradation on the obtained data. All pulse radiolysis experiments have been performed at room temperature.

Dose per single pulse was determined by measurement of 5 mM solution of KSCN, saturated with N_2O, followed at 480 nm (ε = 7600 dm^3 mol^{-1} cm^{-1}) for the formation of $(SCN)_2^{\bullet-}$. The assumed radiation-chemical yield of thiocyanate reaction with hydroxyl radicals was G = 5.6 × 10^{-7} mol J^{-1}.

Based on dosimetry results, doses in all conducted experiments were determined to be 35–40 Gy per pulse. The uncertainty of dose measurement is up to 10% based on accelerator performance. While the used radiation dose can be considered as relatively high, especially for pulse radiolysis of biomolecules, it was necessary for tracking kinetics of TyrO$^{\bullet}$ formation and decay. Each data point was obtained by averaging 9 (in wavelength-dependent experiments) or 15 (in concentration-dependent experiments) repeated measurements.

2.3. Stochastic simulations

Probabilistic simulations of tyrosyl radical formation were conducted with the use of Kinetiscope software package (Hinsberg and Houle, 2017). Based on the utilization of Gillespie algorithm (Gillespie, 1976), it calculates time profiles of products and substrates concentration for given reaction and order-specific reaction rate constant. Therefore, simulation results can be utilized in confirmation of a reaction mechanism if compared with experimental results.

3. Results and discussion

3.1. Absorption spectra of transient species

Previous observations on tyrosine indicated that the main route of tyrosyl radical formation involves water molecule elimination from hydroxyl radical adduct to the aromatic ring in the tyrosine side chain (the dihydroxycyclohexadienyl radicals, $^{\bullet}$TyrOH, reaction 4) (Land and Ebert, 1967; Lynn and Purdie, 1976). While $^{\bullet}$OH forms adducts at a high rate both in meta- and ortho-positions (reactions 1 and 2, respectively), water elimination has been reported only from the o-adducts. The reported absorption band maximum for m-isomer is located at around 305 nm, while for o-isomer it is 330 nm. Absorbance values at 330 nm are therefore to some degree influenced by the contribution from m-isomer absorption band. Tyrosyl radicals have a characteristic double absorption band with maxima at 390 and 405 nm (Land et al., 1961). The transient spectra for the model tripeptide presented in this work consisted mostly of bands corresponding to reactions of a tyrosine residue. A comparison of the spectra of peptide solution at pH = 5.4 and pH = 3.0 (Fig. 2) shows that H^+ greatly promotes the water elimination reaction. The lower pH limit used for measurement was set at 3.0, to prevent significant changes in the ionic structure of GYG peptide, that could alter the kinetics as the pK_a of a carboxyl group at terminal glycine is around 2.3 (Nozaki and Tanford, 1967) and the isoelectric point of the peptide is 5.9 according to manufacturer's data. Even higher yields of TyrO$^{\bullet}$ can be formed in 50 mM phosphate buffer, which is probably caused by the high ionic strength of the buffer solution and subsequently high proton availability.

The spectral shift of the maximum near 330 nm towards longer wavelengths and broadening of the o- $^{\bullet}$TyrOH band can be caused by overlap with absorption of another transient being the product of reaction with atomic hydrogen. H$^{\bullet}$ reacts with the tyrosine side-group in a similar way as hydroxyl radical, forming radical adduct to the aromatic ring. H-atom adduct to phenol ring has an absorption maximum at 350 nm, according to the reports (Feitelson and Hayon, 1973). The presence of the aforementioned adducts has been confirmed by pulse radiolysis in

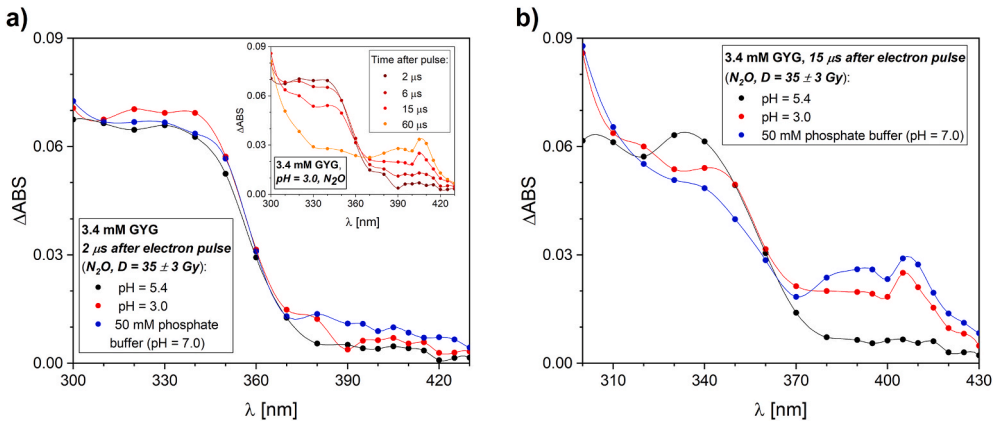

Fig. 2. Absorption spectra of transient species in 3.4 mM solutions of GYG tripeptide: a) 2 μs after electron pulse (inset: evolution of spectrum in time for tripeptide at pH = 3.0); b) 15 μs after electron pulse; all samples saturated with N_2O. Dose per pulse $D = 35 \pm 3$ Gy.

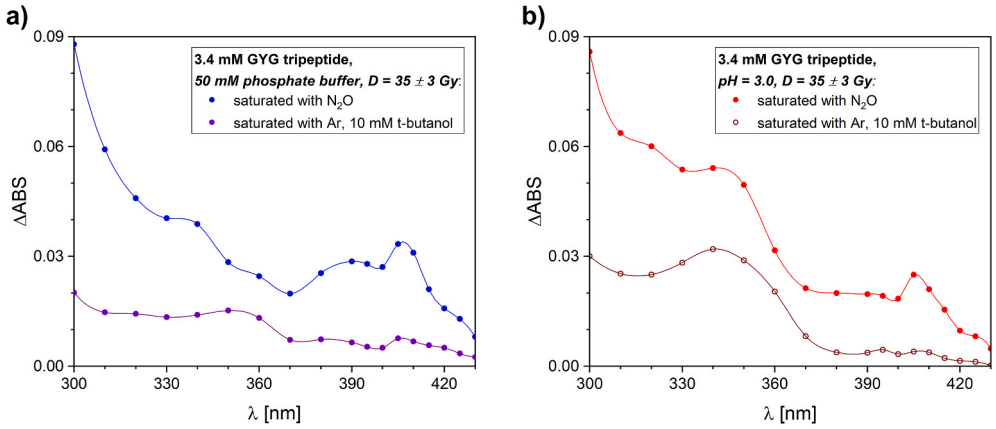

Fig. 3. Comparison between spectra of transients formed in solution during reaction with $^{\bullet}$OH and in the presence of a hydroxyl radical scavenger 15 μs after the electron pulse: a) in 50 mM phosphate buffer (pH = 7.0); b) in water at pH = 3.0. Tripeptide concentration $c = 3.4$ mM, dose per pulse $D = 35 \pm 3$ Gy.

Table 1
Rate constants of formation and decay of radicals formed on tyrosine residue in GYG peptide and their respective acquisition data; k_2 as determined for solution in phosphate buffer. Data compared with values for tyrosine from Solar et al. (1984).

Radical	Reaction rate constant [$dm^3\ mol^{-1}\ s^{-1}$]		Wavelength	Molar absorption coefficient at a given wavelength [$dm^3\ mol^{-1}\ cm^{-1}$]
	Formation	Decay		
Pulse radiolysis results for GYG peptide in phosphate buffer at pH = 7.0				
$^{\bullet}$TyrOH (*ortho*)	$k_2 = (6.0 \pm 0.3)\times10^9$	$k_4 = (6.4 \pm 0.7)\times10^7$ $2k_6 = (2.6 \pm 0.3)\times10^8$	330 nm	3300
TyrO$^{\bullet}$	$k_3 = (6.0 \pm 0.6)\times10^8$ $k_4 = (6.4 \pm 0.6)\times10^7$	$2k_7 = (3.4 \pm 0.2)\times10^8$ $k_8 = (1.7 \pm 0.2)\times10^8$	410 nm	2600
Reaction rate constants for tyrosine at pH = 7.0, buffered with $Ba(OH)_2$ (Solar et al., 1984)				
$^{\bullet}$TyrOH (*ortho*)	$k_2 = (7.0 \pm 0.5)\times10^9$	$k_4 = (1.8 \pm 0.2)\times10^4\ (s^{-1})$ $2k_6 = (3.0 \pm 1.0)\times10^8$	330 nm	3300
TyrO$^{\bullet}$	$k_3 = (6.0 \pm 1.0)\times10^8$ $k_4 = (1.8 \pm 0.2)\times10^4\ (s^{-1})$	$2k_7 = (4.0 \pm 1.0)\times10^8$	405 nm	2600

the presence of tert-butanol serving as hydroxyl radical scavenger (Fig. 3). Further reactions of this H-adduct are not expected to yield tyrosyl radicals.

In acidic solution, the formation of atomic hydrogen is greatly enhanced by the reaction of the hydrated electron with H^+, resulting in a broad and well-defined absorption band at 340 nm. For H-Gly-Tyr-Gly-OH solution in phosphate buffer, change in absorption is lesser and has a maximum at 350 nm. Change at 350 nm does not match any previous reports regarding reactions of phosphate buffer (Rosso et al., 1998), so it can be assumed to follow the same H$^{\bullet}$ mechanism. In the presence of tert-butanol, despite the scavenging of $^{\bullet}$OH, a small fraction of tyrosyl radicals is still formed, similarly to the results obtained for natural pH (Fig. 2). It can be assigned to the fast process of TyrO$^{\bullet}$ formation without observable intermediate product described by Solar (Solar et al., 1984), and while the process (reaction 3) is not very efficient, change of the absorbance is visible due to the relatively high dose used in the measurements.

3.2. Kinetics of reaction with hydroxyl radical and formation of tyrosyl radicals

All reaction rate constants for reactions involved in the reaction of a tyrosine residue in GYG peptide have been shown in Table 1. Molar absorption coefficients are based on the dose-dependent measurements for tripeptide solutions concerning hydroxyl radicals yield, assuming that all absorbance comes only from one type of radicals at a given wavelength and reaction yield does not change within applied dose range. Obtained molar absorption coefficients are equal, within the experimental error, to ones previously reported for L-tyrosine at given wavelengths (Solar et al., 1984). Literature k_4 value is presented as a first-order rate constant, since in the cited study experiments were performed only at pH = 7.0.

The main process towards the formation of tyrosyl radicals is by water elimination from o-adducts of hydroxyl radicals to aromatic ring in the tyrosine side chain (reaction 4). A second-order reaction rate constant for the formation of this type of adducts (reaction 2), $k_2 = (6.1 \pm 0.3)\times10^9$ dm^3 mol^{-1} s^{-1}, was obtained based on spectroscopic measurements from the increase of the adduct band at 330 nm at pseudo-first-order conditions for natural pH of the peptide (Fig. 4). While lowest used concentration of the peptide (85 μM) may be concerning in terms of pseudo-first-order conditions at given dose – being about five times higher than the concentration of hydroxyl radicals, due to high value of reaction rate constant for reactions 1–3, deviation from linearity was not higher than expected based on dose stability. In phosphate buffer solutions, rate constant of this reaction corresponded to $k_2 = (6.0 \pm 0.3) \times10^9$ dm^3 mol^{-1} s^{-1} and at pH = 3.0 was established around $k_2 = (6.6 \pm 0.2)\times10^9$ dm^3 mol^{-1} s^{-1}. All of the obtained values are relatively close to the previously reported $k = (7.0 \pm 0.5) \times10^9$ dm^3 mol^{-1} s^{-1} for this reaction in L-tyrosine (Solar et al., 1984). The value of addition reaction rate constant at low pH was most likely an outcome of overlapping with the absorption band of H-adducts at 350 nm, which could be observed to a lower degree in the case of buffer solution. Water elimination from hydroxyl radical adduct in meta position has not been observed. The addition to the aromatic ring of tyrosine residue both in meta- and ortho- are primary reactions of GYG peptide with hydroxyl radical. The reaction of $^\bullet$OH with glycine residues, not followed here, must have been at least an order of magnitude slower than reaction with tyrosine – with reaction rate constant of $^\bullet$OH with glycine in the used ranges of pH being lower than 1×10^8 dm^3 mol^{-1} s^{-1} (Anbar and Neta, 1967; Štefanić et al., 2001).

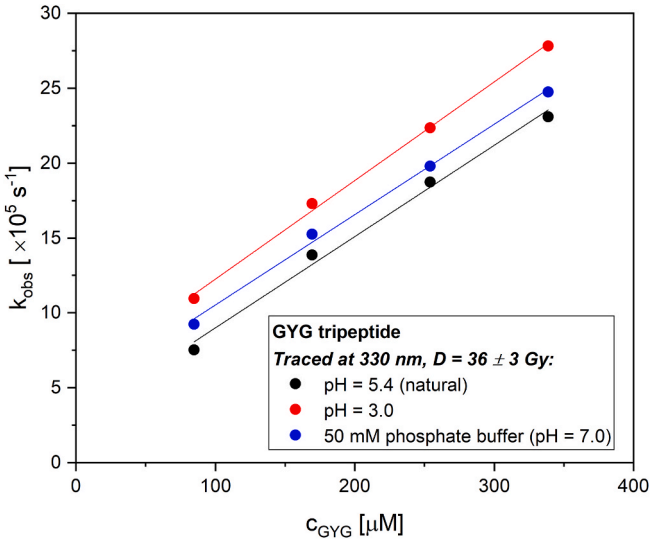

Fig. 4. Pseudo-first-order kinetics of hydroxyl radical addition to tyrosine side-chain in ortho position at different pH and ionic strength conditions tracked at 330 nm. Dose per pulse $D = 36 \pm 3$ Gy.

The decay of adducts formed during the reaction with hydroxyl radicals (Fig. 5a) may result in the formation of DOPA by means of recombination and disproportionation of radicals (reactions 5–6) or may lead to tyrosyl radicals formation after the elimination of water molecule in the presence of protons (reaction 4). The recorded decay in absorbance as a function of time consisted of two kinetically different processes, one of which highly depends on pH, while the other one seems to take place independently. Separation of the water elimination kinetics was achieved by measuring decay rate constants at 330 nm as a function of pH (Fig. 5a). This allowed to calculate the rate constants for pH-dependent decay (reaction 4) and pH-independent process (reaction 6).

Time-resolved measurements of tyrosyl radicals were conducted at 410 nm to minimize the potential effects of spectral band overlap. The deconvolution of the recorded signals for two exponential growth functions showed contributions from the pH/buffer-independent TyrO$^\bullet$ formation (reaction 3) and also water elimination reaction to the buildup of the 410 nm band (reaction 4) corresponding to the H$^+$-catalyzed decay of o-dihydroxycyclohexadienyl radicals.

The second-order reaction rate constant of the formation of phenoxyl radicals without observable transient product (reaction 3) was $k_3 = (6.0 \pm 0.6)\times10^8$ dm^3 mol^{-1} s^{-1}, which is the exact value previously reported in the literature for tyrosine (Getoff, 1992). This process may be the effect of hydroxyl radical attack in ipso position with hydrogen atom transfer (Yamabe and Yamazaki, 2018), and while relatively fast when compared to water elimination reaction, it is highly ineffective due to competition with an order of magnitude faster reactions of $^\bullet$OH addition in positions ortho and meta.

Reaction leading to tyrosyl radicals formation via water elimination could be tracked both from growth at 410 nm and decay at 330 nm, which helped distinguish it from the kinetics of other competing processes, such as recombination and disproportionation of $^\bullet$TyrOH. The observed pseudo-first order reaction rate constants linearly changed with the ratio of $^\bullet$TyrOH to H$^+$ present in solutions (Fig. 5a). Based on that, the second-order rate constant was calculated as $k_4 = (6.4 \pm 0.7)\times10^7$ dm^3 mol^{-1} s^{-1} for H$^+$-catalyzed water elimination reaction. The same value for this reaction rate constant was obtained for growth at 410 nm. By determining the reaction rate constant of water elimination, the reaction rate constant of $k_6 = (2.6 \pm 0.3)\times10^8$ dm^3 mol^{-1} s^{-1} was calculated for other processes involved in the decay of $^\bullet$TyrOH. The calculations for water elimination reaction did not include the samples with theoretically low concentration of available H$^+$ i.e. samples with pH = 5.4. Relatively low concentration of observed phenoxyl radicals in those samples, as well as possible contribution of terminal carboxylic group of the peptide to total H$^+$ available for reaction or possibility of spontaneous water elimination without H$^+$ contribution cause kinetic results deviate from other conditions taken into consideration in the study.

The decay of tyrosyl radicals observed at 410 nm may possibly be caused by a multitude of hard-to-distinguish reactions, with estimated reaction rate constants of $k_7 = (3.4 \pm 0.2)\times10^8$ dm^3 mol^{-1} s^{-1} for reactions between two tyrosyl radicals and $k_8 = (1.7 \pm 0.2)\times10^8$ dm^3 mol^{-1} s^{-1} for other involved processes, which was mathematically best fit for observed decay in all measured samples. Recombination and disproportionation reactions are expected to occur between two TyrO$^\bullet$ and also between phenoxyl radicals and other radicals present in the irradiated solution, i.e. reaction of TyrO$^\bullet$ and $^\bullet$TyrOH leading to tyrosine recovery with elimination of water has been suggested before (Lynn and Purdie, 1976; Boguta and Dancewicz, 1981). Presence of oxygen in the system even in trace amounts can lead to reactions of dihydroxycyclohexadienyl radicals with O_2 ($k \approx 10^8$-10^9 dm^3 mol^{-1} s^{-1}) and phenoxyl radicals with $HO_2^\bullet$ or $O_2^{\bullet-}$ ($k = 1.7\times10^9$ dm^3 mol^{-1} s^{-1}) (Hunter et al., 1989; Getoff, 1992), which further complicates the analysis of reactions leading to radicals decay in the investigated systems.

The results obtained from pulse radiolysis of buffered solutions with various phosphates concentrations (Fig. 6a) indicated that the enhanced yield of tyrosyl radicals formation is the result of the high availability of protons – kinetic processes observed at 330 nm and 410 nm directly

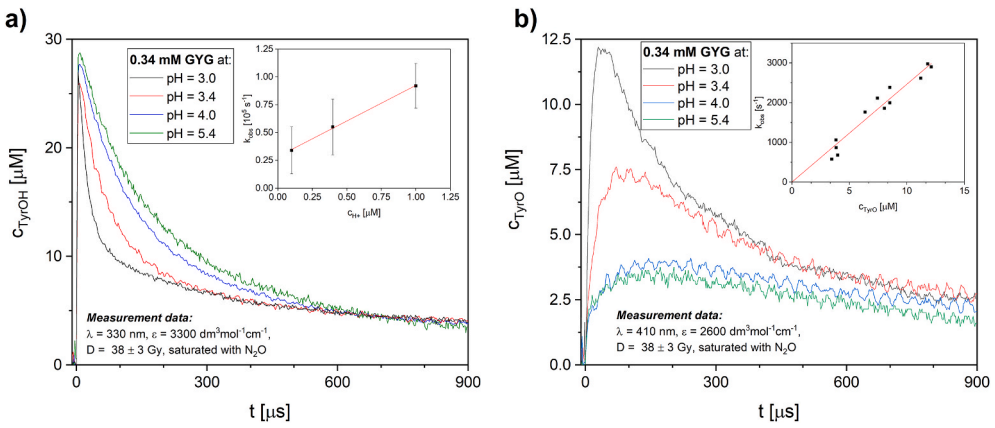

Fig. 5. a) Kinetic traces of decay of hydroxyl radical adducts to tyrosine aromatic ring, recorded at 330 nm for solutions of various pH, peptide concentration $c = 0.34$ mM, dose per pulse $D = 38 \pm 3$ Gy, $\varepsilon = 3300$ dm^3 mol^{-1} cm^{-1} (Inset: observed first-order reaction rate constant for $^{\bullet}$TyrOH decay at 330 nm as a function of H^+ concentration). b) Formation and decay of tyrosyl radicals at various pH, tracked at 410 nm, $c = 0.34$ mM, dose per pulse $D = 38 \pm 3$ Gy, $\varepsilon = 2600$ dm^3 mol^{-1} cm^{-1} (Inset: observed reaction rate constant of decay plotted against maximum concentrations of TyrO$^{\bullet}$).

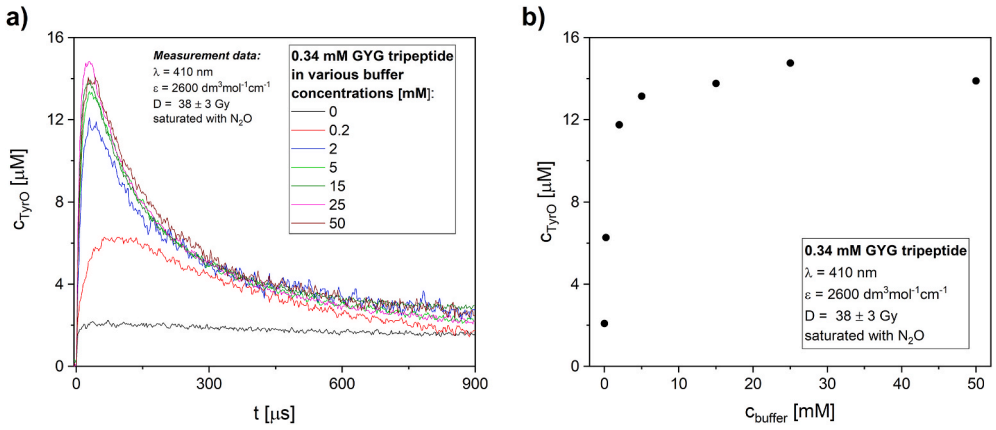

Fig. 6. a) Formation and decay of tyrosyl radicals (concentrations calculated from kinetic traces at 410 nm, $\varepsilon = 2600$ dm^3 mol^{-1} cm^{-1}) for various phosphate buffer concentrations, pH = 7.0, peptide concentration c = 0.34 mM, dose per pulse $D = 38 \pm 3$ Gy; b) Maximum concentration of tyrosyl radicals as a function of phosphate buffer concentration, conditions as above.

correspond to the ones observed at low pH. In the peptide solutions (0.34 mM) with increasing buffer concentration, maximum observed concentration of TyrO$^{\bullet}$ raises up to 15 μM and subsequently levels off at ca. 10 mM of the buffer (Fig. 6b). Similarities to kinetics observed in samples at pH = 3 suggest that phosphate buffer serves as reversible source of protons for water elimination reaction leading to formation of TyrO$^{\bullet}$. Dependence of phenoxyl radicals formation in function of phosphate buffer concentration is limited by availability of hydroxyl radical adducts.

Table 2
List of reactions taken into consideration during calculations and their respective reaction rate constants.

Reaction	Reaction rate constant [dm^3 mol^{-1} s^{-1}]	Source
$H_2O \rightarrow {}^{\bullet}OH, H^{\bullet}, e^-_{aq}$	Dose-dependent parameters[a]	–
$2\ {}^{\bullet}OH \rightarrow H_2O_2$	$2k = 1.1\times10^{10}$	Buxton et al. (1988)
$H^{\bullet} + {}^{\bullet}OH \rightarrow H_2O$	$k = 7.0\times10^{9}$	
$e^-_{aq} + H^+ \rightarrow H^{\bullet}$	$k = 2.3\times10^{10}$	
$e^-_{aq} + N_2O \rightarrow {}^{\bullet}OH$	$k = 9.1\times10^{9}$	
Tyrosine + $^{\bullet}$OH → $^{\bullet}$TyrOH	$k_2 = 6.0\times10^{9}$	This study
Tyrosine + $^{\bullet}$OH → TyrO$^{\bullet}$	$k_3 = 6.0\times10^{8}$	
$^{\bullet}$TyrOH + H^+ → TyrO$^{\bullet}$	$k_4 = 6.4\times10^{7}$	
2 $^{\bullet}$TyrOH → products	$2k_6 = 2.6\times10^{8}$	
2 TyrO$^{\bullet}$ → products	$2k_7 = 3.4\times10^{8}$	
TyrO$^{\bullet}$ + $^{\bullet}$TyrOH → products	$k_8 = 1.7\times10^{8}$	

[a] Parameters providing a linear generation of radicals for the duration of the electron pulse (17 ns)

3.3. Stochastic simulations of tyrosyl radicals formation

The initial model used for calculations was developed by utilizing reactions predicted in the mechanism of TyrO$^{\bullet}$ formation and decay, adding known recombination reactions of water radiolysis products (considering their contribution to simulation results). The final qualitative model includes the formation of main water radiolysis products by 17 ns electron pulse, recombination between formed radicals, reactions of tyrosine with hydroxyl radical, and water elimination from $^{\bullet}$OH adduct (Table 2).

While rate constants were obtained experimentally and used in simulations to confirm the coherence of the postulated mechanism of tyrosyl radicals formation, they also had proven to be a valuable tool to assess the possible pathways of TyrO$^{\bullet}$ decay. There are most likely other processes contributing to observed reaction rate constants k_6, k_7, and k_8, but based on fit to experimental data (Fig. 6), disproportionation reactions between TyrO$^{\bullet}$ and $^{\bullet}$TyrOH is of considerable significance.

The results of stochastic calculations (Fig. 7) are in reasonably good agreement with the experimental data obtained for the corresponding samples at pH 3.0, 3.4 and 4.0, as well as for samples with the addition of buffer. Difference observable between the sample at pH = 4.0 and the one in 0.2 mM phosphate buffer (Fig. 7c) may be caused by multiple overlapping effects – possible carboxylic group deprotonation contribution to water elimination process, which would be different for buffer-

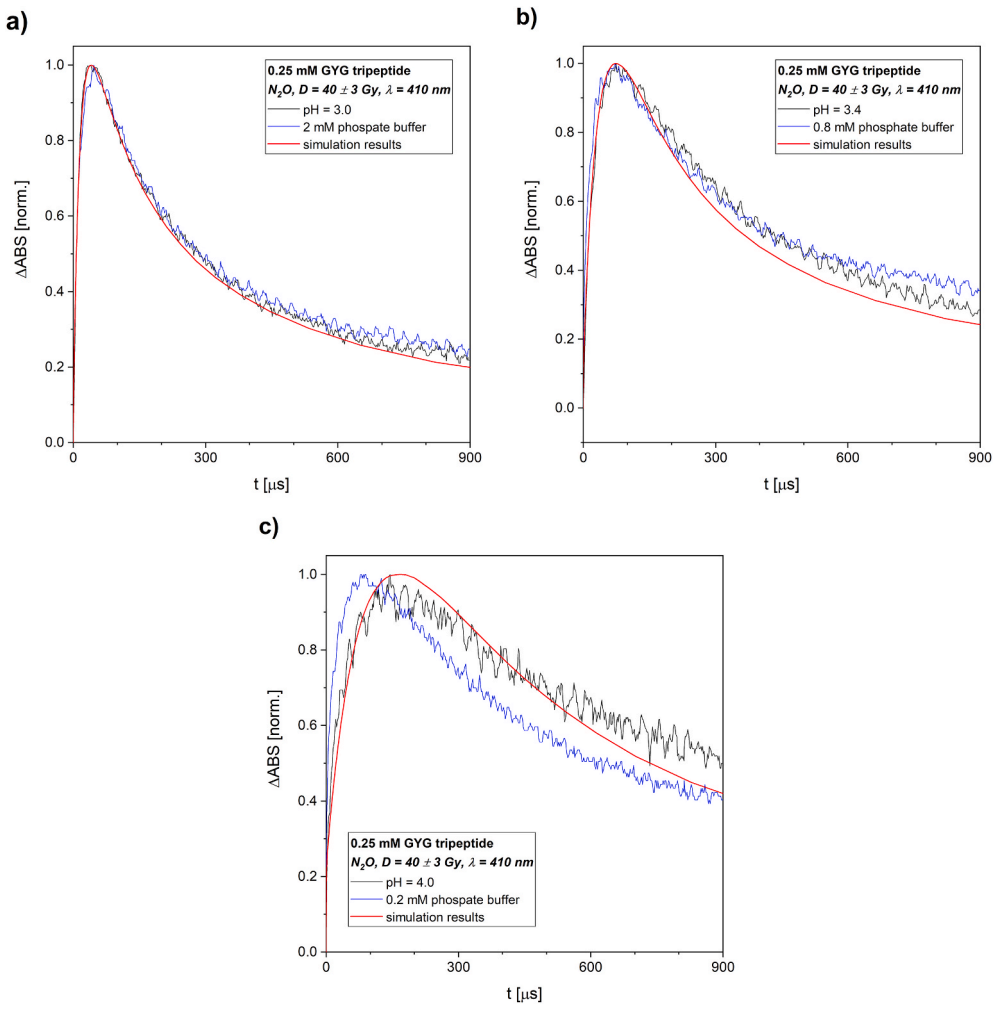

Fig. 7. a-c) Normalized absorbance of phenoxyl radicals at 410 nm in comparison with corresponding stochastic simulation results. Peptide concentration $c = 0.25$ mM, dose per pulse $D = 40 \pm 3$ Gy.

and acid- containing samples, as well as contribution of relatively low concentration of TyrO$^{\bullet}$ which emphasize measurement uncertainty (trace amount of oxygen and dose fluctuations). Due to differences in dissociation constants of buffer salts, only monobasic sodium phosphate was assumed to serve as source of protons available for reaction. Therefore, the concentration of H^+ used for stochastic calculations was assumed as a half of the buffer concentration. Results show that the mechanism includes all reactions significantly contributing to the formation of phenoxyl radicals.

4. Conclusions

Hydroxyl radicals react with GYG tripeptide mainly by addition to the tyrosine ring. Replacing the carboxyl and amino terminal functions in tyrosine by peptide bonds does not significantly influence the reaction pathways and kinetics known from earlier works on pure tyrosine. Pulse radiolysis experiments confirmed that phenoxyl radicals on tyrosine residues are formed primarily through water elimination from hydroxyl radical adduct to the ring, which is catalyzed by the presence of H^+. Changes in reaction environment (use of buffer, change of pH) have a significant influence only on kinetics and yield of water elimination reaction that leads to TyrO$^{\bullet}$ formation. Based on the kinetic data and simple stochastic simulations it is possible to predict the yield of phenoxyl radicals based on amount of H^+ available for reaction. The mechanistic scheme has been confirmed by demonstrating agreement of kinetic simulation results with experimental observations.

While lowering the pH of the solution greatly promotes the yield of TyrO$^{\bullet}$, it can potentially complicate reaction mechanisms by protonation of peptide or protein, and also by increasing the formation of highly reactive atomic hydrogen. Using buffer as a source of protons for the reaction may be an alternative, since according to the presented results it does not change the mechanism of the reaction compared to the use of acid. This observation may be also important in terms of peptides and proteins radiolysis – buffers are widely used in sample preparation.

Author statement

Sebastian Sowiński: investigation, formal analysis, visualization, methodology, writing (original draft preparation); **Gustavo H. C. Varca**: conceptualization, funding acquisition, resources, writing (reviewing & editing); **Sławomir Kadłubowski**: validation, writing (reviewing & editing); **Ademar B. Lugão:** supervision, writing (reviewing & editing); **Piotr Ulański**: methodology, supervision, writing (reviewing & editing).

Declaration of competing interest

The authors declare that they have no known competing financial interests or personal relationships that could have appeared to influence the work reported in this paper.

Acknowledgements

The authors would like to thank Sao Paulo Research Foundation - FAPESP for a scholarship (No. 2010/10935-9 2015-13979-0), the International Atomic Energy Agency IAEA (CRP F22064) and Conselho Nacional de Desenvolvimento Cientifico e Tecnologico (CNPq) (project no. 402887/2013-1) for financial support.

References

Amri, E., Mamboya, F., 2012. Papain, a plant enzyme of biological importance: a review. Am. J. Biochem. Biotechnol. 8 (2), 99–104.

An, J.-C., Weaver, A., Kim, B., Barkatt, A., Poster, D., Vreeland, W.N., Silverman, J., Al-Sheikhly, M., 2011. Radiation-induced synthesis of poly(vinylpyrrolidone) nanogel. Polymer 52 (25), 5746–5755. https://doi.org/10.1016/j.polymer.2011.09.056.

Anbar, M., Neta, P., 1967. A compilation of specific bimolecular rate constants for the reactions of hydrated electrons, hydrogen atoms and hydroxyl radicals with inorganic and organic compounds in aqueous solution. Int. J. Appl. Radiat. Isot. 18 (7), 493–523. https://doi.org/10.1016/0020-708X(67)90115-9.

Bian, S., Chowdhury, S.M., 2014. Profiling protein-protein interactions and protein structures using chemical cross-linking and mass spectrometry. Austin J. Biomed. Eng. 1 (4), 1017.

Boguta, G., Dancewicz, A.M., 1981. Radiation-induced dimerization of tyrosine and glycyltyrosine in aqueous solutions. Int. J. Radiat. Biol. Relat. Stud. Phys. Chem. Med. 39 (2), 163–174. https://doi.org/10.1080/09553008114550181.

Buxton, G.V., Greenstock, C.L., Helman, W.P., Ross, A.B., 1988. Critical review of rate constants for reactions of hydrated electrons, hydrogen atoms and hydroxyl radicals (·OH/·O−) in aqueous solution. J. Phys. Chem. Ref. Data 17 (2), 513–886. https://doi.org/10.1063/1.555805.

Dispenza, C., Sabatino, M.A., Grimaldi, N., Bulone, D., Bondì, M.L., Casaletto, M.P., Rigogliuso, S., Adamo, G., Ghersi, G., 2012. Minimalism in radiation synthesis of biomedical functional nanogels. Biomacromolecules 13 (6), 1805–1817. https://doi.org/10.1021/bm3003144.

Duygu Sütekin, S., Güven, O., 2019. Application of radiation for the synthesis of poly(N-vinyl pyrrolidone) nanogels with controlled sizes from aqueous solutions. Appl. Radiat. Isot. 145, 161–169. https://doi.org/10.1016/j.apradiso.2018.12.028.

Fazolin, G.N., Varca, G.H.C., Kadlubowski, S., Sowinski, S., Lugão, A.B., 2020. The effects of radiation and experimental conditions over papain nanoparticle formation: towards a new generation synthesis. Radiat. Phys. Chem. 169 https://doi.org/10.1016/j.radphyschem.2018.08.033, 107984.

Feitelson, J., Hayon, E., 1973. Electron ejection and electron capture by phenolic compounds. J. Phys. Chem. 77 (1), 10–15. https://doi.org/10.1021/j100620a003.

Gaber, M.H., 2005. Effect of γ-irradiation on the molecular properties of bovine serum albumin. J. Biosci. Bioeng. 100 (2), 203–206. https://doi.org/10.1263/jbb.100.203.

Getoff, N., 1992. Pulse radiolysis of aromatic amino acids—state of the art. Amino Acids 2 (3), 195–214. https://doi.org/10.1007/BF00805942.

Gillespie, D.T., 1976. A general method for numerically simulating the stochastic time evolution of coupled chemical reactions. J. Comput. Phys. 22 (4), 403–434.

Giulivi, C., Traaseth, N.J., Davies, K.J.A., 2003. Tyrosine oxidation products: analysis and biological relevance. Amino Acids 25 (3), 227–232. https://doi.org/10.1007/s00726-003-0013-0.

Hägglund, P., Mariotti, M., Davies, M.J., 2018. Identification and characterization of protein cross-links induced by oxidative reactions. Expet Rev. Proteonomics 15 (8), 665–681. https://doi.org/10.1080/14789450.2018.1509710.

Heinecke, J.W., Li, W., Francis, G.A., Goldstein, J.A., 1993. Tyrosyl radical generated by myeloperoxidase catalyzes the oxidative cross-linking of proteins. J. Clin. Invest. 91 (6), 2866–2872. https://doi.org/10.1172/JCI116531.

Hinsberg, W., Houle, F., 2017. Kinetiscope: a stochastic kinetics simulator. http://hinsberg.net/kinetiscope/.

Houée-Levin, C., Bobrowski, K., 2013. The use of the methods of radiolysis to explore the mechanisms of free radical modifications in proteins. J. Proteom. 92, 51–62. https://doi.org/10.1016/j.jprot.2013.02.014.

Hunter, E.P.L., Desrosiers, M.F., Simic, M.G., 1989. The effect of oxygen, antioxidants, and superoxide radical on tyrosine phenoxyl radical dimerization. Free Radic. Biol. Med. 6 (6), 581–585. https://doi.org/10.1016/0891-5849(89)90064-6.

Kamphuis, I.G., Kalk, K.H., Swarte, M.B.A., Drenth, J., 1984. Structure of papain refined at 1.65 Å resolution. J. Mol. Biol. 179 (2), 233–256. https://doi.org/10.1016/0022-2836(84)90467-4.

Karolczak, S., Hodyr, K., Połowiński, M., 1992. Pulse radiolysis system based on ELU-6E Linac—II. Development and upgrading the system. Int. J. Radiat. Appl. Instrum. C Radiat. Phys. Chem. 39 (1), 1–5. https://doi.org/10.1016/1359-0197(92)90162-9.

Land, E.J., Ebert, M., 1967. Pulse radiolysis studies of aqueous phenol. Water elimination from dihydroxycyclohexadienyl radicals to form phenoxyl. Trans. Faraday Soc. 63, 1181–1190. https://doi.org/10.1039/TF9676301181.

Land, E.J., Porter, G., Strachan, E., 1961. Primary photochemical processes in aromatic molecules. Part 6.—the absorption spectra and acidity constants of phenoxyl radicals. Trans. Faraday Soc. 57, 1885–1893. https://doi.org/10.1039/TF9615701885.

Lynn, K.R., Purdie, J.W., 1976. Some pulse and gamma radiolysis studies of tyrosine and its glycyl peptides. Int. J. Radiat. Phys. Chem. 8 (6), 685–689. https://doi.org/10.1016/0020-7055(76)90041-3.

Matusiak, M., Kadlubowski, S., Rosiak, J.M., 2020. Nanogels synthesized by radiation-induced intramolecular crosslinking of water-soluble polymers. Radiat. Phys. Chem. 169 https://doi.org/10.1016/j.radphyschem.2018.12.019, 108099.

Müller, A., Barat, S., Chen, X., Bui Cuong, K., Bozko, P., Malek, N.P., Plentz, R.R., 2016. Comparative study of antitumor effects of bromelain and papain in human cholangiocarcinoma cell lines. Int. J. Oncol. 48 (5), 2025–2034. https://doi.org/10.3892/ijo.2016.3411.

Nozaki, Y., Tanford, C., 1967. Acid-base titrations in concentrated guanidine hydrochloride. Dissociation constants of the guanidinium ion and of some amino acids. J. Am. Chem. Soc. 89 (4), 736–742. https://doi.org/10.1021/ja00980a002.

Queiroz, R.G., Varca, G.H.C., Kadlubowski, S., Ulanski, P., Lugão, A.B., 2016. Radiation-synthesized protein-based drug carriers: size-controlled BSA nanoparticles. Int. J. Biol. Macromol. 85, 82–91. https://doi.org/10.1016/j.ijbiomac.2015.12.074.

Rosso, J.A., Rodríguez Nieto, F.J., Gonzalez, M.C., Mártire, D.O., 1998. Reactions of phosphate radicals with substituted benzenes. J. Photochem. Photobiol. Chem. 116 (1), 21–25. https://doi.org/10.1016/S1010-6030(98)00266-4.

Saha, A., Mandal, P.C., Bhattacharyya, S.N., 1995. Radiation-induced inactivation of enzymes—a review. Radiat. Phys. Chem. 46 (1), 123–145. https://doi.org/10.1016/0969-806X(94)00130-C.

Solar, S., Solar, W., Getoff, N., 1984. Reactivity of hydroxyl with tyrosine in aqueous solution studied by pulse radiolysis. J. Phys. Chem. 88 (10), 2091–2095. https://doi.org/10.1021/j150654a030.

Soto Espinoza, S.L., Sánchez, M.L., Risso, V., Smolko, E.E., Grasselli, M., 2012. Radiation synthesis of seroalbumin nanoparticles. Radiat. Phys. Chem. 81 (9), 1417–1421. https://doi.org/10.1016/j.radphyschem.2011.11.040.

Štefanić, I., Bonifačić, M., Asmus, K.-D., Armstrong, D.A., 2001. Absolute rate constants and yields of transients from hydroxyl radical and H atom attack on glycine and methyl-substituted glycine anions. J. Phys. Chem. 105 (38), 8681–8690. https://doi.org/10.1021/jp011975o.

Ulański, P., Janik, I., Rosiak, J.M., 1998. Radiation formation of polymeric nanogels. Radiat. Phys. Chem. 52 (1), 289–294. https://doi.org/10.1016/S0969-806X(98)00155-8.

Ulański, P., Kadłubowski, S., Rosiak, J.M., 2002. Synthesis of poly(acrylic acid) nanogels by preparative pulse radiolysis. Radiat. Phys. Chem. 63 (3), 533–537. https://doi.org/10.1016/S0969-806X(01)00549-7.

Ulanski, P., Rosiak, J.M., 2004. Polymeric nano/microgels. In: Nalwa, H.S. (Ed.), Encyclopedia of Nanoscience and Nanotechnology, vol. VIII. American Scientific Publishers, pp. 845–871.

Varca, G.H.C., Kadlubowski, S., Wolszczak, M., Lugão, A.B., Rosiak, J.M., Ulanski, P., 2016. Synthesis of papain nanoparticles by electron beam irradiation – a pathway for controlled enzyme crosslinking. Int. J. Biol. Macromol. 92, 654–659. https://doi.org/10.1016/j.ijbiomac.2016.07.070.

Varca, G.H.C., Perossi, G.G., Grasselli, M., Lugão, A.B., 2014. Radiation synthesized protein-based nanoparticles: a technique overview. Radiat. Phys. Chem. 105, 48–52. https://doi.org/10.1016/j.radphyschem.2014.05.020.

Yamabe, S., Yamazaki, S., 2018. A DFT study of proton transfers for the reaction of phenol and hydroxyl radical leading to dihydroxybenzene and H_2O in the water cluster. Int. J. Quant. Chem. 118 (6) https://doi.org/10.1002/qua.25510 e25510.